

Supporting Information to:

**Facile method for fabrication of buckled PDMS silver nanorods arrays as active 3D SERS cage for bacterial sensing**

Samir Kumar<sup>a</sup>, Devesh K Lodhi,<sup>a</sup> Pratibha Goel<sup>a</sup>, Neeti<sup>b</sup>, Prashant Mishra<sup>b</sup>, J. P. Singh<sup>\*,a</sup>

<sup>a</sup> *Department of Physics, Indian Institute of Technology Delhi, Hauz Khas, New Delhi 110016, India*

<sup>b</sup> *Department of Biochemical Engineering and Biotechnology, Indian Institute of Technology Delhi, Hauz Khas, New Delhi 110016, India*

\* To whom correspondence should be addressed. Electronic mail: [jpsingh@physics.iitd.ac.in](mailto:jpsingh@physics.iitd.ac.in)

## A. Experimental Section

**PDMS Substrate Preparation:** The PDMS substrate (~1 mm thickness) was prepared by mixing a prepolymer (Sylgard 184, Dow Corning) with a curing agent in a 10:1 ratio at room temperature. The mixture was then poured on ultrasonically acetone cleaned Si wafer and was cured at 85 °C for 20 min.

**SERS substrate preparation:** The silver nanorods (AgNRs) were obliquely deposited over stretched PDMS films by thermal evaporation of silver powder (99.9%) using glancing angle deposition (GLAD) method and this state after the growth of AgNRs on the stretched PDMS will be called prestretched AgNRs-PDMS substrate. For silver nanorods formation, the stretched PDMS were inclined in such a way that the substrate normal made a very high angle ( $\alpha = 85^\circ$ ) with respect to the direction of incident vapor flux.<sup>1,2</sup> During the initial growth of the films, the impinging atoms form isolated nucleation centers which cast shadow for the arriving vapor flux.<sup>3,4</sup> The nucleated islands act as shadowing centers and hence the larger nucleation centers will receive more impinging atoms as compared to the smaller ones and only the larger islands will grow. The competition between limited adatom surface mobility and shadowing effect results in the evolution of the columnar structure with the growth of Ag nanorods in the direction of the incident vapor flux. During deposition the substrates were at room temperature and the pressure of the deposition chamber was better than  $2 \times 10^{-6}$  Torr.

**Preparation of bacterial culture:** *P. aeruginosa* (MTCC 2453) was grown for 16 hours in 10 mL of Luria-Bertani broth at 37 °C and 220 rpm. Cells were harvested during the late log phase by centrifugation at 8000 rpm for 10 minutes. Subsequently,  $10^8$  Cells were taken and washed 3 to 4 times with deionized (DI) Millipore water.

**SERS measurements:** After deposition the AgNR-PDMS substrate were taken out from the chamber. The cell pellet of *P. aeruginosa* was re-suspended in 0.5 mL of water. The 3  $\mu$ L of the resulting bacterial suspension was pipetted directly onto the SERS substrate, dried at ambient temperature and pressure before the data analysis. SERS spectra were acquired using a micro Raman system (Horiba LabRAM HR Evolution). After SERS measurement of *P. aeruginosa* on the stretched AgNR-PDMS substrate the strain of the sample was released slowly. SERS

measurement were repeated after releasing strain of the AgNR-PDMS substrate. Laser was focused into sample by Olympus infinity corrected objective lens (100X, 1.4 NA). A 514 nm argon ion laser was used for excitation with 20 mW output (1 mW at the sample surface). The acquisition time was 20 s. SERS spectra over the range of 400  $\text{cm}^{-1}$  – 1800  $\text{cm}^{-1}$  were collected from 5 randomly selected spots across the substrate. All measurements were done at room temperature and 520  $\text{cm}^{-1}$  band of silicon was used for the frequency calibration.

**SERS Substrate characterization:** Film morphology and structural analysis were performed using scanning electron microscope (SEM, ZEISS EVO 50). Figure S1 shows the SEM micrograph of Ag nanorods arrays deposited on the unstretched PDMS film substrate.

### B. Table T1 Raman band assignments of *P. aeruginosa*

Wave number ( $\text{cm}^{-1}$ )	Component	Assignment	References
674	DNA	Ring Breathing (G)	5, 6
730	DNA	Ring Breathing (A)	5, 6
1010	Protein	Ring Breathing (Phe)	6, 7
1052	Protein	Phe	6
1110	Nucleic Acids		11
1152	Carotenoids	Carotene –C–H– stretch	8, 10, 12
1066	Lipids		12
1090	Protein	Amide III	12
1238	Protein	Amide III ( $\beta$ strand)	6, 7, 9
1323	Protein	Amide III	6, 7
1433	Protein/lipids	$\text{CH}_2$ – $\text{CH}_3$ bend	6, 9, 12
1484	DNA	Ring mode (G, A)	5, 6
1510	Carotenoids	Carotene –C=H– stretch	8, 10, 12
1576	Protein	Phe	6
1608	Protein	Tyr	4, 9

Abbreviations: G, guanine; A, adenine; P, Phe, phenylalanine; Tyr, tyrosine

The peaks between 500-1100  $\text{cm}^{-1}$  is due to various other groups present in the bacteria.

### C. Additional Figures

**Figure S1:** (a) SEM image of the Ag nanorods arrays grown over PDMS film. (b) Effect of mechanical strain ( $\epsilon= 30\%$ ) on AgNR-PDMS film morphology (c) Higher magnification SEM images of the corresponding surfaces. The SEM micrographs clearly show that the final sample consists of dual scale roughness due to micron-sized wrinkles of PDMS and nanoscale roughness of Ag nanorods.

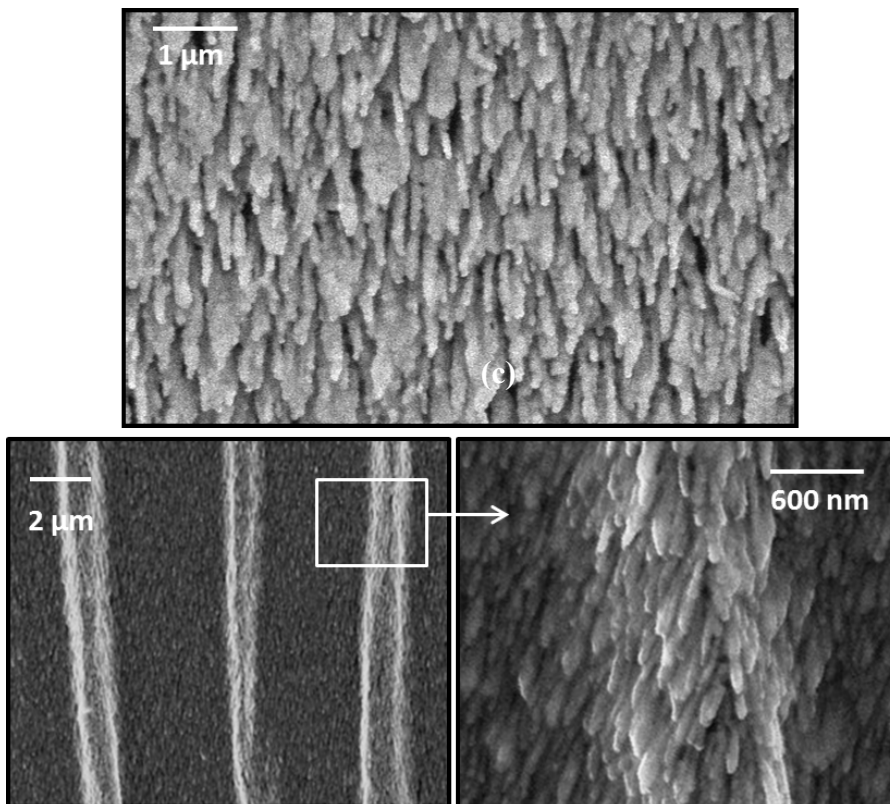


**Figure S2:** Raman Spectra of bare AgNR-PDMS substrate.

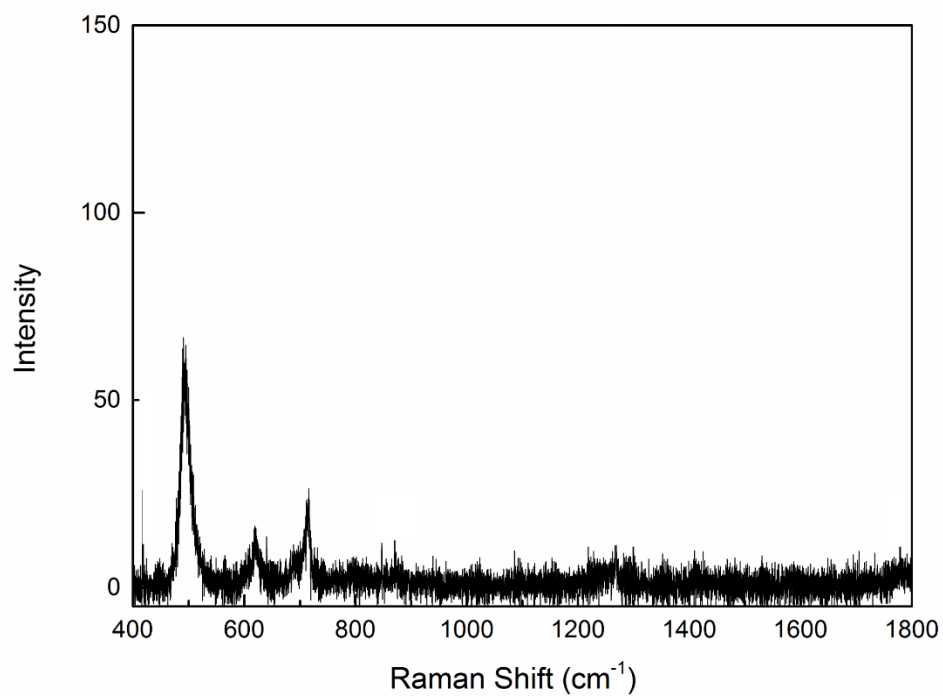


**Figure S3:** The effect of stress cycle on Raman enhancement. Increment in the SERS signal,  $f$  versus stress-release cycle.

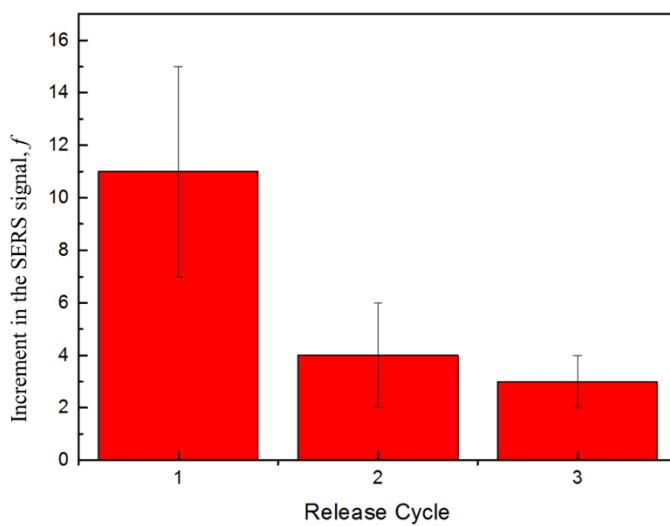


**Figure S4:** The spectra of two different samples of *P. aeruginosa* (prepared and measured at different weeks). We see that the differences between the two spectra appear to be rather small, though one cannot entirely rule out that some secondary differences are present. Although the spectra in Fig. S4 are similar and the reproducibility is good, there are some differences in the major bands in the region 1300-1500  $\text{cm}^{-1}$ . This region can be expected to involve the groups that have the strongest interaction with the silver surface. It is likely that slight variations in the parameters such as the concentration of bacteria, the concentration of Ag, and the time of adsorption affect this interaction and alter the spectrum.

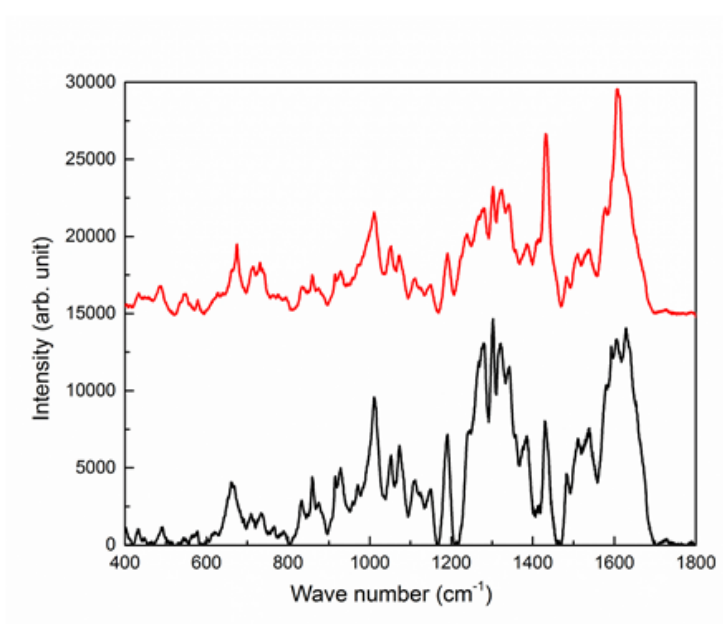
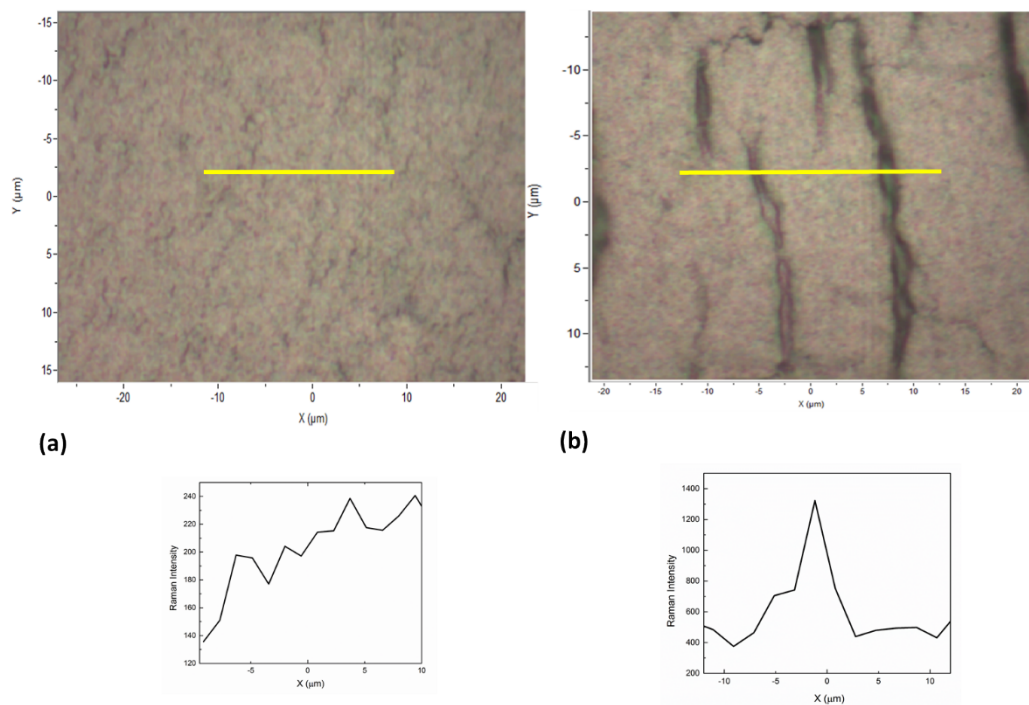
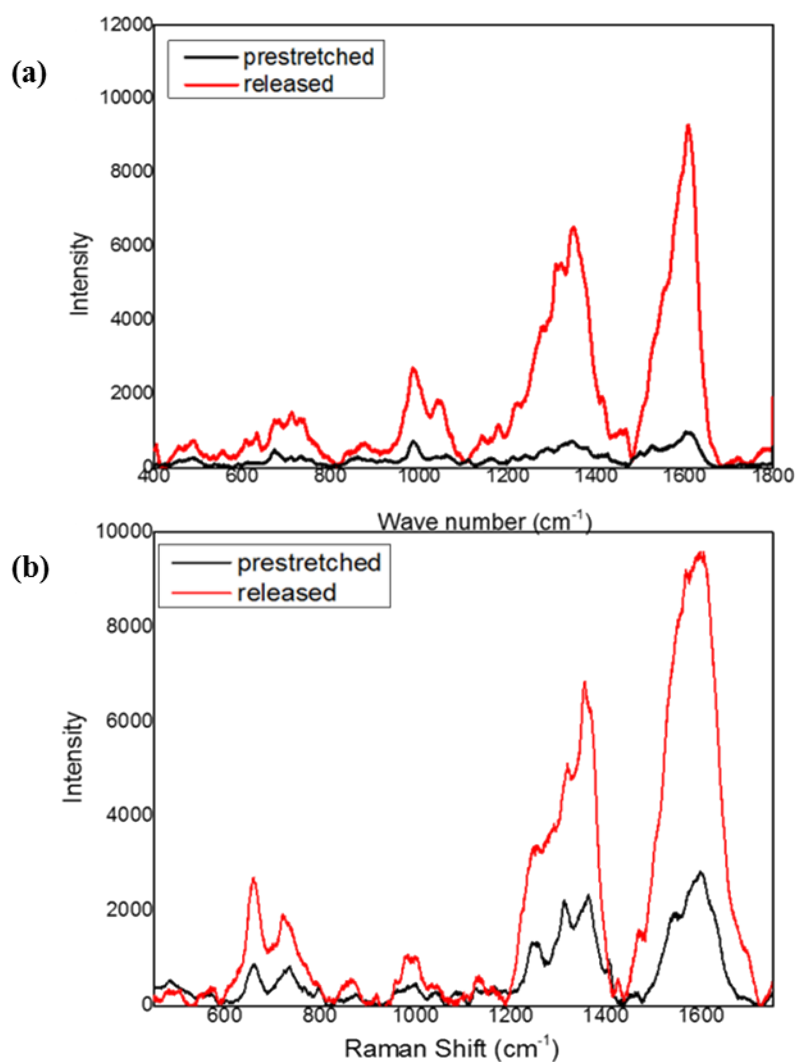


**Figure S5:** Optical images and Line Profile of the characteristic  $1605\text{ cm}^{-1}$  on AgNR-PDMS substrate (a) in stretched position (b) after releasing the stress.



Two things can be observed from the figure. First, the Raman counts are very high (in thousands) in case of the wrinkled substrate, as compared to that of stretched AgNR-PDMS substrate. Second, for wrinkled substrate, there is a huge variation in Raman peak that depends upon the position.

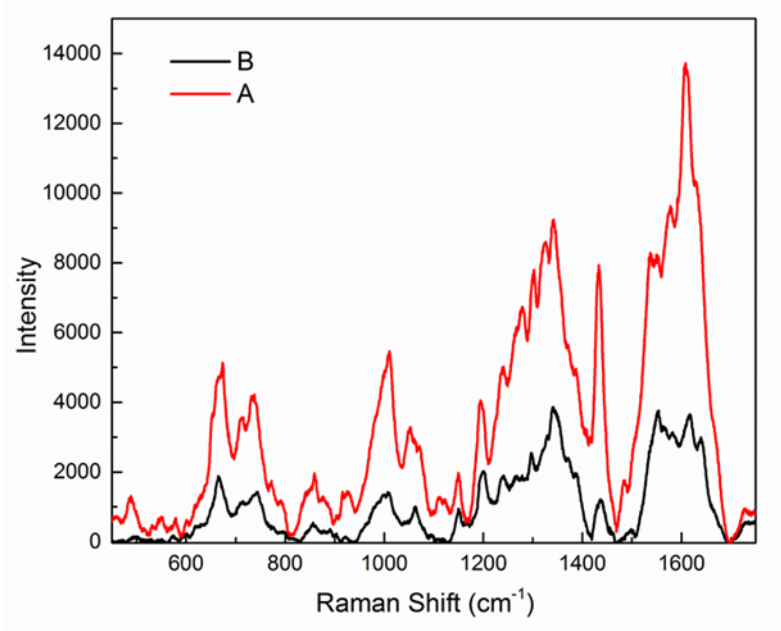
**Figure S6:** Raman spectra of (a) *Bacillus* and (b) *E. Coli* before and after releasing the strain.



The Raman spectra of *Bacillus*, which is a Gram- positive bacteria and *E. Coli* which is a Gram- Negative bacteria. The cell wall of *Bacillus* is very different than that of Gram- negative *P. aeruginosa* or *E. Coli*. The SERS of the three bacteria share a number of similar features. For example bands near 730 cm<sup>-1</sup>, 1350 cm<sup>-1</sup>, and 1608 cm<sup>-1</sup> can be identified in SERS spectra in Fig 7. It is now widely accepted that an inherent biochemical mechanism of these bacterial cells

contribute to the observed SERS bacterial signature.<sup>13</sup> There is a slight differences in the spectra of the three bacterial samples in the regions  $500\text{-}650\text{ cm}^{-1}$ ,  $700\text{-}750\text{ cm}^{-1}$  and  $900\text{-}1000\text{ cm}^{-1}$ . The slight differences may be attributed to the structural differences in the cell wall.<sup>14,15</sup>

**Figure S7:** Raman spectra of *P. aeruginosa* (A) releasing the stress after dropping the bacteria on the stretched AgNR-PDMS substrate, (B) first releasing the stress of the AgNR-PDMS substrate and then dropping the bacteria.



## D. Finite-Difference Time-Domain (FDTD) Modeling

FDTD is a time propagation algorithm, which integrates the Maxwell's curl equations in time domain. The electric field vector can be calculated at any arbitrary point of the simulation geometry and time. The incident laser beam used in our experiments was unpolarized. In FDTD the external source excitations are polarized in a particular direction. We performed the simulations with two mutually orthogonal polarization called as “s” and “p” polarization and found that the electric field on the surface of nanorods changes slightly, so we are showing simulation results only for “p” polarization. Our simulation geometries are approximation of the real geometries shown in the SEM images. The flat substrate with nanorods was modeled as two dimensional array of nanorods arranged in a 2-D rhombic Bravais lattice with separation of  $L_x =$

500 nm in x-direction and  $L_y = 160$  nm in y-direction on the PDMS substrate. The buckled substrate was modeled as a curved surface with the staggered nanorods array having  $L_x = 500$  nm and,  $L_y = 130$  nm.  $L_x$  is reduced to 130 nm because of the nanorods density increase after the formation of buckles shown in the SEM images. The nanorods on average have length  $\sim 930$  nm, diameter  $\sim 110$  nm and make an angle of  $\sim 65^\circ$  with the substrate normal. Figures are showing the morphologies used in simulation for flat as well as buckled substrate. These geometries are discretized with the cell edge  $< 8$  nm and the time step is chosen to be  $< 10^{-17}$  seconds resulting from the Courant stability condition, which ensures the stability for the plane wave excitation with 511 nm wavelength. In case of the flat geometry the periodic boundary condition is employed in both x and y-direction to extend the geometry to infinite. Incident wave is traveling in negative z-direction, the perfectly matched layer boundary condition is employed on the upper and lower boundary of the simulation geometry. In case of curved geometry the periodic boundary condition is employed on the both ends in x direction and perfectly matched layer is employed in the y and z direction of the computational space. The permittivity of Ag material is implemented according to the Drude model,

$$\varepsilon(\omega) = 1 - \frac{\omega_p^2}{\omega(i\gamma + \omega)}$$

where  $\omega_p (= 1.37 \times 10^{16}$  rad/s) is the plasma frequency and  $\gamma (= 2.73 \times 10^{13}$  rad/s) is the scattering frequency for the bulk Ag, in case of nanorods the scattering frequency is increased by a factor of 3 to consider the increased scattering in case of nanorods. The relative permittivity for the PDMS substrate is taken to be 1.42.

## References

- 1 T. Karabacak, J. P. Singh, Y.-P. P. Zhao, G.-C. C. Wang and T.-M. M. Lu, *Phys. Rev. B*, 2003, **68**, 125408.
- 2 M. T. Taschuk, M. M. Hawkeye and M. J. Brett, *Glancing Angle Deposition*, Elsevier Ltd., Third Edit., 2010.
- 3 D. P. Singh, P. Goel and J. P. Singh, *J. Appl. Phys.*, 2012, **112**, 104324.

- 4 C. Khare, C. Patzig, J. W. Gerlach, B. Rauschenbach and B. Fuhrmann, *J. Vac. Sci. Technol. A Vacuum, Surfaces, Film.*, 2010, **28**, 1002.
- 5 J. De Gelder, K. De Gussem, P. Vandenabeele and L. Moens, *J. Raman Spectrosc.*, 2007, **38**, 1133–1147.
- 6 J. M. Benevides, M. Tsuboi, J. K. Bamford and G. J. Thomas, *Biophys. J.*, 1997, **72**, 2748–62.
- 7 R. Tuma, J. H. K. Bamford, D. H. Bamford and G. J. Thomas, Jr, *J. Mol. Biol.*, 1996, **257**, 102–115.
- 8 G. J. Puppels, H. S. Garritsen, J. A. Kummer and J. Greve, *Cytometry*, 1993, **14**, 251–6.
- 9 J. G. Grasselli, M. K. Snavely and B. J. Bulkin, *Chemical applications of Raman spectroscopy*, Wiley, New York, 1981.
- 10 M. Scholtes-Timmerman, H. Willemse-Erix, T. B. Schut, A. van Belkum, G. Puppels and K. Maquelin, *Analyst*, 2009, **134**, 387–93.
- 11 C. Sandt, T. Smith-Palmer, J. Pink and D. Pink, *Appl. Spectrosc.*, 2008, **62**, 975–983.
- 12 G. Rusciano, P. Capriglione, G. Pesce, P. Abete, V. Carnovale and A. Sasso, *Laser Phys. Lett.*, 2013, **10**, 075603.
- 13 W. R. Premasiri, Y. Gebregziabher and L. D. Ziegler, *Appl. Spectrosc.*, 2011, **65**, 493–9.
- 14 L. Zeiri, B. V Bronk, Y. Shabtai and J. Cze, *Colloids Surfaces A Physicochem. Eng. Asp.*, 2002, **208**, 357–362.
- 15 A. Sengupta, M. L. Laucks, N. Dildine, E. Drapala and E. J. Davis, *J. Aerosol Sci.*, 2005, **36**, 651–664.